Yunfei Xing
State Key Laboratory of
High Temperature Gas Dynamics,
Institute of Mechanics,
Chinese Academy of Sciences,
Beijing 100190, China

Fengquan Zhong[1]
State Key Laboratory of
High Temperature Gas Dynamics,
Institute of Mechanics,
Chinese Academy of Sciences,
Beijing 100190, China;
School of Engineering Science,
University of Chinese Academy of Sciences,
Beijing 100049, China
e-mail: fzhong@imech.ac.cn

Xinyu Zhang
State Key Laboratory of
High Temperature Gas Dynamics,
Institute of Mechanics,
Chinese Academy of Sciences,
Beijing 100190, China;
School of Engineering Science,
University of Chinese Academy of Sciences,
Beijing 100049, China

Numerical Study of Impingement Cooling of Aviation Kerosene at Supercritical Conditions

In the present paper, numerical study of flow and heat transfer properties of RP-3 kerosene at liquid and supercritical conditions in an impingement model is conducted with renormalization group (RNG) $k-\varepsilon$ turbulence model and a ten-species surrogate of kerosene. The independence of grids is first studied, and the numerical results are compared with experimental data for validation. Characteristics of flow and heat transfer of kerosene flow in the impingement model are studied with different inlet mass flow rates and different inlet temperatures. The velocity and temperature field show similar profile compared to that of air impingement. The heat transfer rates increase first with the increasing of inlet temperature and then decrease suddenly when the inlet temperature is 500 K.
[DOI: 10.1115/1.4040612]

Keywords: impingement cooling, supercritical condition, heat transfer, kerosene

1 Introduction

Active cooling using hydrocarbon fuels as coolant is one of the most effective ways for rocket and scramjet applications. To limit the weight of the cooling system, regenerative cooling using onboard fuel as the primary coolant is considered to be the most effective way for thermal management. The fuel state before entering the combustor varies with different operation conditions. In the early (low-speed) stage for a liquid-hydrocarbon-fueled scramjet, because the amount of heat absorbed by the fuel is minimal, the hydrocarbon fuel would remain in the liquid state. As the flight speed increases, the fuel temperature may exceed its thermodynamic critical temperature, and the fuel can become supercritical when the fuel pressure is also supercritical. Flow and heat transfer properties of hydrocarbon fuels in circular or rectangular cooling channels have been widely studied via heating facility [1–3] or numerical simulations [4–6]. Many of previous studies on heat transfer of hydrocarbon fuels are focused on supercritical and fully developed pipe flows. For example, Linne and Meyer [4] studied supercritical heat transfer and high-temperature pyrolysis of JP7 kerosene with electrical heating pipe system. Hu et al. [5] experimentally investigated heat transfer of kerosene at high wall heat fluxes and identified heat transfer deterioration in the region close to the critical point of kerosene. Zhong et al. [6] studied characteristics of heat transfer of kerosene at low to moderate wall heat fluxes by using a multiple-stage heating facility and discussed the process of heat transfer deterioration and enhancement during the phase change. Dang et al. [7] numerically studied turbulent flow and convective heat transfer of kerosene at supercritical conditions in a straight tube. The results showed that flow properties such as velocity and Reynolds number increase significantly along the axial direction as the fuel temperature rises and heat transfer of kerosene undergoes deterioration when wall heat flux exceeds a critical value.

It is known that for rocket or scramjet combustor, local peaks of heat flux exist due to extensive combustion and local flow structures. For example, for a Mach 2.5 supersonic combustor, local heat flux may reach 3–4 MW/m^2, which is at least three times of the averaged wall heat flux [8]. The commonly used convective heat transfer is no longer able to absorb heat from the wall efficiently and keep the wall temperature within the safe range. Therefore, effective cooling concepts are required for these highly loaded components. Impinging jets, due to their ability to achieve high heat and mass transfer rates, have been widely used in gas turbine cooling applications such as the cooling of turbine vanes and blades, and combustor liners [9–12]. Numerous investigations on flow and heat transfer characteristic of air multiple jet impingement [13–15] have published the effect of impingement hole shape, size, and locations on heat transfer coefficient and its uniformity. Several reviews that have published on the impingement subject, respectively, aimed at summarizing the latest developments in impingement technology, measurement technique, and numerical computations [16–19].

However, most of previous studies on impingement jet cooling are focused on gaseous or simple liquid jets. To the authors' acknowledgments, study of impingement jet of aviation kerosene especially at supercritical conditions has not been reported yet. Thermodynamic and transport properties of the ten-component kerosene proposed in Ref. [6] by our previous study show density and viscosity of kerosene decrease remarkably in the vicinity of the critical point as functions of temperature and pressure. It is expected that flow and heat transfer properties of supercritical kerosene would exhibit unique characteristics due to significant changes in the thermodynamic and transport properties. More details of variations in thermodynamic and transport properties of supercritical kerosene can be found in Ref. [6]. The objective of the paper is to investigate heat transfer properties and pressure loss for kerosene impingement cooling at supercritical condition. Although the results in literature mentioned above provide insights into both the convective heat transfer of kerosene flows in pipe at supercritical conditions and properties of the air impingement cooling, the combination of the impingement configuration and supercritical aviation kerosene in the present study is unique.

[1]Corresponding author.
Contributed by the Heat Transfer Division of ASME for publication in the JOURNAL OF HEAT TRANSFER. Manuscript received January 10, 2018; final manuscript received June 4, 2018; published online July 23, 2018. Assoc. Editor: Amy Fleischer.

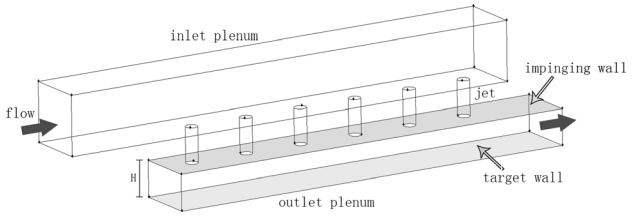

Fig. 1 The sketch up of the impingement model

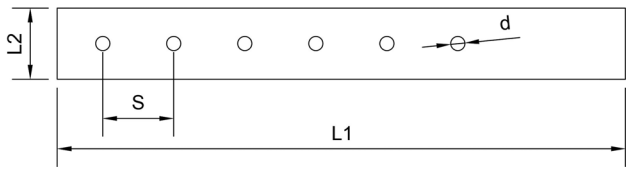

Fig. 2 The configuration of impinging wall

2 Geometry and Parameters of Impingement Configuration

Kerosene flow in an impingement model having six impinging jets with the diameter of 1 mm is studied with numerical method. The impingement model is shown in Fig. 1 and the configuration of the impinging wall is shown in Fig. 2. The flow enters the inlet plenum followed by the six impinging jets generated by an impingement plate, and the flow exits the outlet plenum after impinging on the target wall. The diameter of jet is 1 mm, the jet-to-jet spacing S is 5 mm, the width of the target wall is 5 mm, the length of the target wall is 35 mm, and the jet-to-wall height H is 3 mm. The kerosene flow is fully turbulent since the inlet Reynolds number is much larger than the critical value of 2300 for turbulent pipe flow. The gravity effect is not included in the present study since the ratio of Grashof number to the square of Reynolds number is smaller than 0.01. Note that for China RP-3 aviation kerosene, pyrolysis occurs and needs to be considered when the fuel temperature reaches approximately 800–850 K at a pressure range of 3–5 MPa [20]. Hence, heat transfer data analyzed in the paper are limited in the flow region where the wall and the fuel temperatures are both below 850 K.

In the impingement system, we define a Reynolds number based on the jet diameter and jet velocity and ΔP is the pressure difference between inlet and outlet.

And the heat transfer coefficient h is defined as follows:

$$h = \frac{Q_w}{T_f - T_w}$$

3 Numerical Method

The Reynolds-averaged Navier–Stokes equations are solved by finite volume method with second-order upwind scheme applied for convective terms and second-order central scheme for viscous terms. The renormalization group (RNG) k–ε model is applied for turbulence modeling and the Wolfstein turbulence model [21] is adopted in the near-wall region characterized with low Reynolds number properties. An outflow boundary condition is applied to the outlet. The heat flux on the target wall is kept as 1 MW/m^2. The SIMPLE algorithm is employed to resolve the coupling between velocity and pressure. The implicit Gauss–Seidel iteration is used to calculate the time advancement. Stretched meshes are used in the near-wall region and a minimum mesh spacing from the wall is kept to be less than 2 in the wall units as given as follows:

$$y^+ = \frac{u_\tau \Delta y}{\nu} < 2$$

with u_τ representing the shear velocity, Δy is the distance of the first grid layer from the wall.

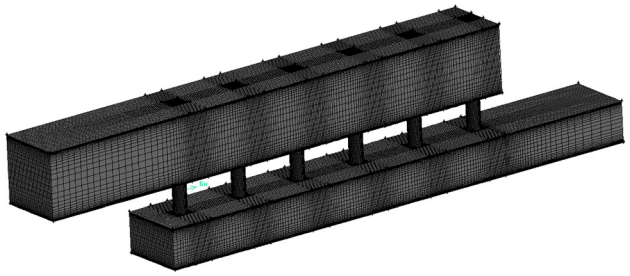

Fig. 3 Numerical grid used in the computational fluid dynamics analysis

The numerical grid used in the computational fluid dynamics analysis is shown in Fig. 3.

A ten-species surrogate of aviation kerosene proposed in our previous study [6] is applied with the extended corresponding state method to determine the thermophysical properties of kerosene such as density, specific heat, viscosity as functions of temperature and pressure. It is found that properties of kerosene change dramatically in the vicinity of the critical point, which attributes to many unique flow and heat transfer phenomena of supercritical kerosene flow as discussed in the literatures [6].

3.1 Grid Independence. A grid independence study has been carried out for the validation of the present numerical method. Three meshes are studied. The total grids numbers are 300,000 (case a), 480,000 (case b), and 600,000 (case c), respectively. We focus on the data on target plate; therefore, the first layer mesh on the target plate is the only varied parameter here, as shown in Table 1. The results of grid-independence study are also reported in Table 1. There is a significant variation between results of case a and case b due to the refined resolution of the viscous sublayer of turbulent boundary layer. The difference of Nusselt number is less than 3% for case b and case c. However, the computational time for case c is nearly two times higher than that of case b. Therefore, case b is applied for all the simulations in the present study.

3.2 Comparison With Experimental Heat Transfer Data. The present numerical method is also validated by comparison of calculated heat transfer coefficient of impingement jet flow with experimental data. It is better to compare results of kerosene impingement jet flow to the experiments directly. However, heat transfer results of impingement jet of kerosene flow at supercritical conditions have not been reported yet. Therefore, air impingement heat transfer is computed with the present numerical method here. The local heat transfer distributions in present impingement system are compared with the experimental data [22] with Reynolds number of 35,000, as shown in Fig. 4. There is a good agreement between the experimental and numerical results. Note that the experimental data are from nine jets system and the exit rims were different from the present paper. Hence, one can see the last jet causes different heat transfer distribution. The peaks values can also be verified by the classical single jet experimental data [23,24]. Figure 5 shows a row-by-row comparison of the area averaged Nu number of the target plate with Florschuetz et al. [25] correlation, which was confirmed by Bailey and Bunker [26]. At Reynolds number of 35,000, agreement is obtained to be within approximately 5%. At the same time, the identical numerical method has been validated by comparing the calculated results

Table 1 Mesh parameters and grid independence results

Case	y^+	h
a	4.3	15,539.2
b	1.27	17,271.1
c	0.8	17,782.9

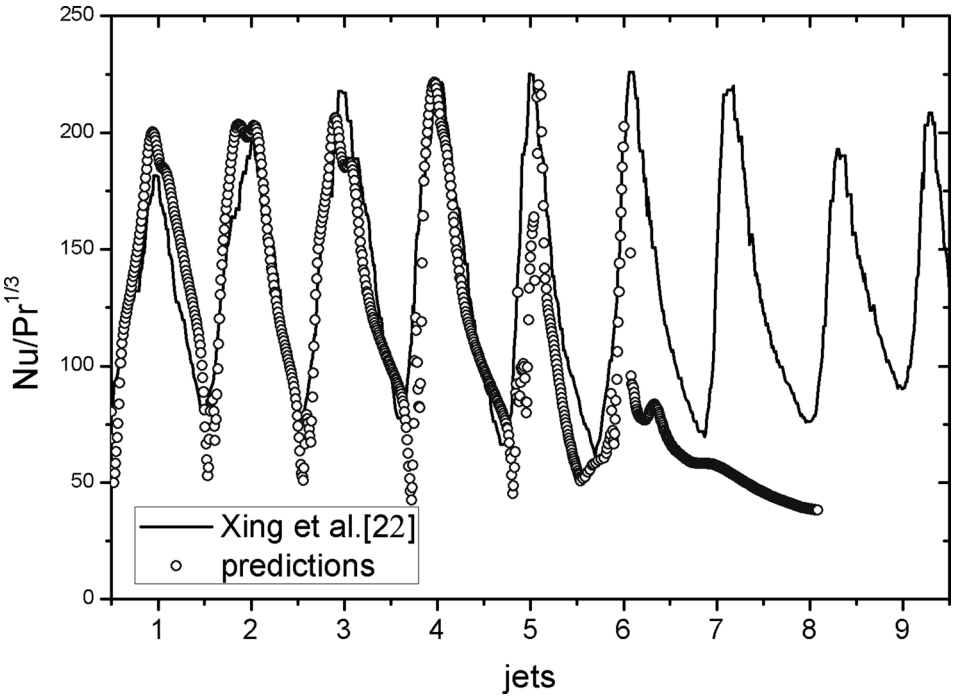

Fig. 4 Comparison of the local Nusselt number distributions with the experimental data [22]

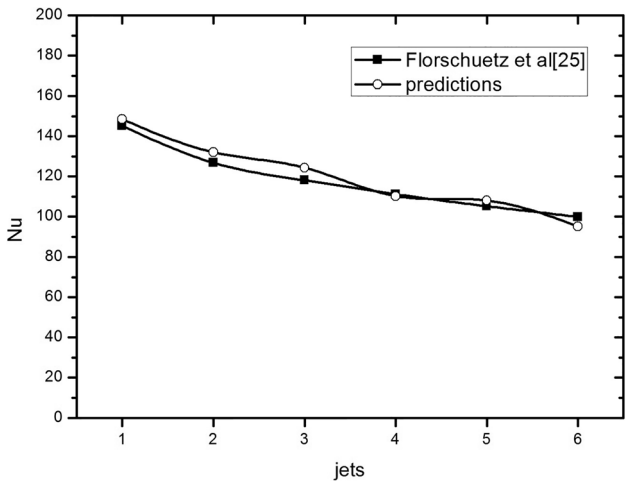

Fig. 5 Comparison with Florschuetz's [25] correlation in different jet rows

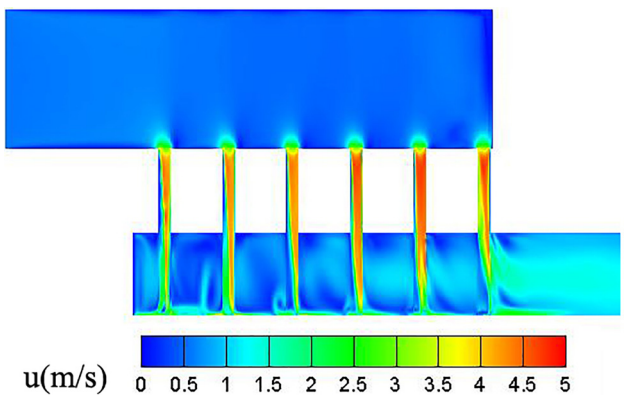

Fig. 6 The magnitude of velocity distribution at the center cross section in the impingement model

with the experimental data of supercritical aviation kerosene in straight circular pipe, and the comparison results are given in our previous work [7].

4 Results and Discussions

Here, aviation kerosene is selected as working fluid. The inlet temperature of the standard case is 400 K, the inlet pressure is 5 MPa, and the heat flux on the target wall is kept as 1 MW/m^2. The inlet mass flow rate of a standard case is 10 g/s (one usually uses the mass flow rate instead of Reynolds number, as the parameters for the cooling of scramjet application).

4.1 Description of the Magnitude of Velocity Distribution. Figure 6 presents the velocity magnitude field at the central x–y plane of the impingement model as shown in Fig. 2. The velocity distribution with each jet is slightly different, and it might be the reason of nonuniform distribution of mass flow caused by the direction of crossflow. Annerfeldt et al. [27] also showed that there exists a pressure drop large enough to result in an uneven distribution of the mass flow over the jet rows and thus, lower Reynolds numbers occur at the first rows. It can be seen that the flow impinges on the target plate with high speed after through the impinging jets. Due to shear layer expansion, interaction between two adjacent jets occurs before the impingement. This interaction would weaken the jet strength and degrade the heat transfer enhancement of jet array.

The local jet mass flow distribution of the present prediction results is compared with the data evaluated based on the one-dimensional (1D) model of Florschuetz et al. [25] as shown in Fig. 7. The predictions of local jet mass flows are calculated by integrating the jet velocity profile at the orifice exit. In general, there is a good agreement between the predictions and the 1D model. The predictions obtained mass flow variations are about 2–4% lower than the 1D model for the first three jets and are about 2–3% higher than the 1D model for the last three jets.

The local jet mass flow distribution and the development of the generated crossflow (G_{cf}) are evaluated based on 1D model of Florschuetz et al. [25]. It has been verified that G_{cf} for a given

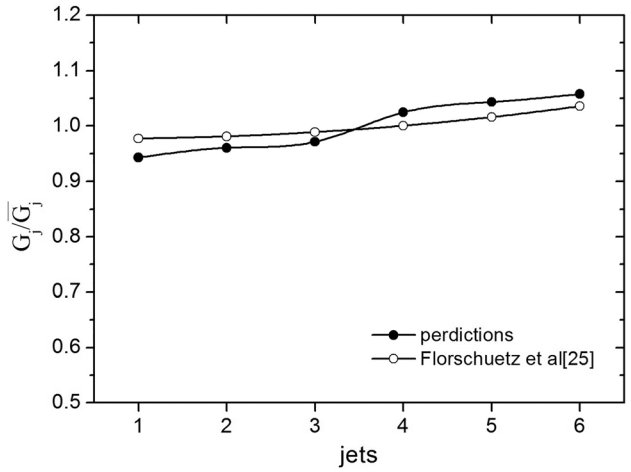

Fig. 7 Jet massflow distribution

discharge depends only on the number of streamwise impingement jets and the channel flow area. Terzis [28] and Florschuetz and Isoda [29] reported that G_{cf} does not affect the discharge of the downstream jets. Here, constant discharge coefficients of $C_D = 0.85$ are determined based on Florschuetz et al. [30]. The crossflow development evaluated with the model of Florschuetz et al. [25] is shown in Fig. 8. One can see that the local crossflow-to-jet mass velocity ratio increases toward the channel exit and highest ratio is below 0.27, which means the crossflow momentum in the present setup is relatively small. Figure 9 shows instantaneous streamlines in cross sections at each jet location. The significant secondary flow is clearly shown in the figures, which affects heat transfer rates on the target wall. Along the exit flow, the secondary flow weakens in the streamwise direction.

4.2 Heat Transfer Distribution on the Target Plate. Figure 10 shows the temperature fields at each jet cross section. One can see that the temperature increases along the streamwise direction (x direction) as kerosene flow accumulates toward the exit. This growing crossflow has significant impacts on the heat transfer of the last two jets on the target plate.

Figure 11 shows contours of heat transfer coefficient on the target wall. The positions of the impingement jets are clearly visible in the heat transfer pattern on the target plate. At the stagnation points, the heat transfer coefficient is highest due to the thin boundary layer. After the jets impinge on the target plate, heat transfer coefficient decreases quickly toward the sides due to the

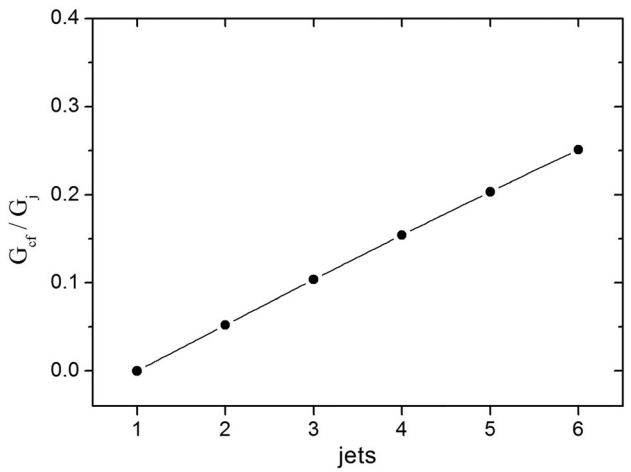

Fig. 8 Crossflow development evaluated with the model of Florschuetz et al. [25]

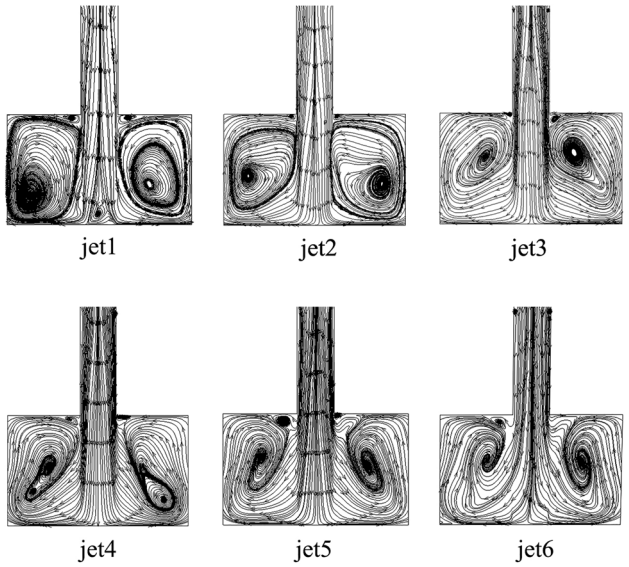

Fig. 9 Distribution of streamlines at each jet location

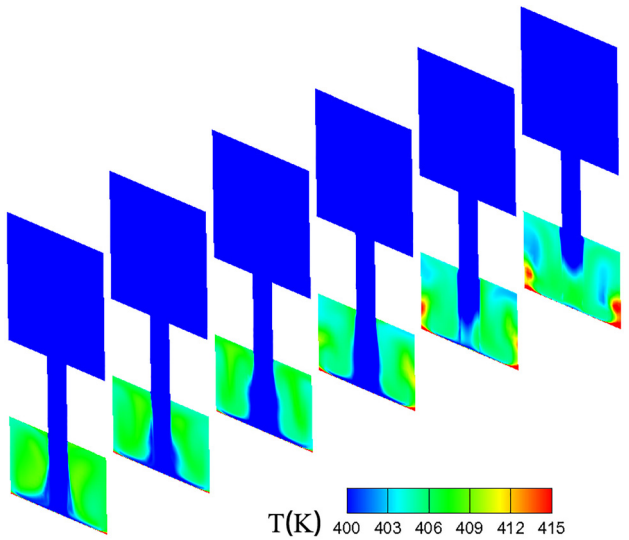

Fig. 10 Temperature fields on each jet cross section along the flow direction

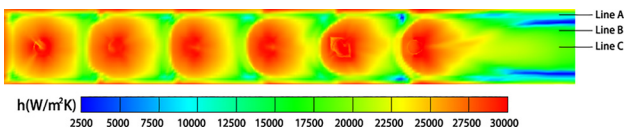

Fig. 11 Heat transfer coefficients distribution on the target wall

decrease of the jet radial velocity with increasing distance from the jet impingement point. Compared to the result of heat transfer coefficient (HTC) for air impingement jets [22], heat transfer coefficient of aviation kerosene impingement shows a similar distribution.

For a quantitative comparison, distributions of heat transfer coefficient along different x-lines (indicated in Fig. 11) are shown in Fig. 12. Here, arrows indicate the locations of impingement jets. Distribution of HTC of each impingement jet is very similar, except the HTC peak decreases slightly as flow approaches the exit. Comparison of distributions of HTC at the three different

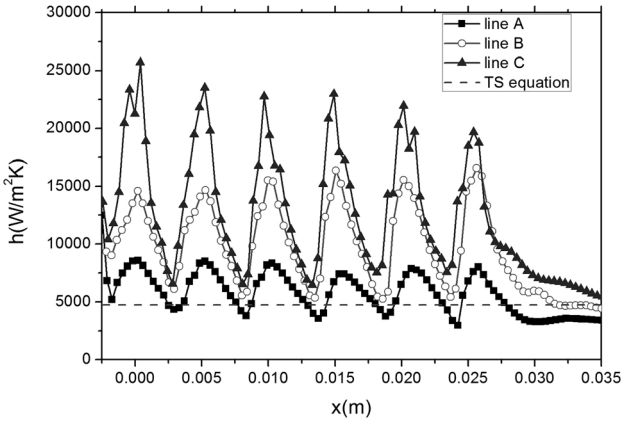

Fig. 12 Distribution of heat transfer coefficient along different *x*-lines on the target wall

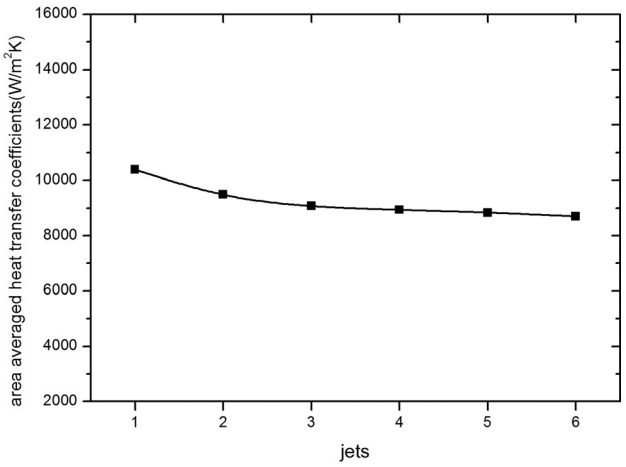

Fig. 13 The area averaged heat transfer coefficients of each jets

spanwise locations indicates that HTC decreases significantly along the spanwise direction since strength of vortices and jet impact on the target plate weaken, where it is far away from the jet core region. Note that the dashed line indicates the value of heat transfer coefficient determined by the classic Tate–Sieder formula for a fully developed channel flow with a diameter equaling to the jet-to-plate height H and with the same mass flow rate. It is obvious that the impingement jets significantly enhance heat transfer on the target plate compared to convective heat transfer of a fully developed channel flow. The area averaged heat transfer coefficients are compared with each jet as shown in Fig. 13. One can see that the area averaged heat transfer coefficients with each jet are decreasing slightly with the increasing of crossflow.

4.3 Effect of Inlet Mass Flow Rate. Figure 14 shows HTC distributions on the target wall with different inlet mass flow rates. One can see that overall, heat transfer coefficient increases with the increasing inlet mass flow rate. It is known that for air or gaseous impingement cooling, heat transfer coefficient can be scaled with $Re^{0.8}$ and the heat transfer coefficient ratios are nearly identical for different Reynolds numbers. Therefore, for aviation kerosene impingement cooling, the ratio of heat transfer coefficients to $Re^{0.8}$ at the line C is given in Fig. 15. In general, the heat transfer ratios are nearly identical for different inlet mass flow rates except that of the first two jets near the left-side wall, which attributes to the effect of the left-side wall and locally larger pressure drop as discussed in the literatures of Annerfeldt et al. [27] and Xing et al.

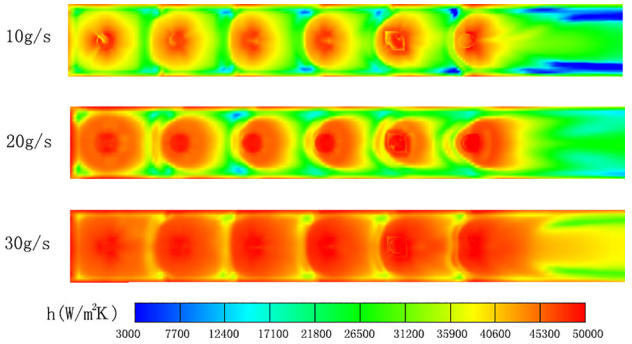

Fig. 14 Heat transfer distributions on the target wall with different mass flow rates

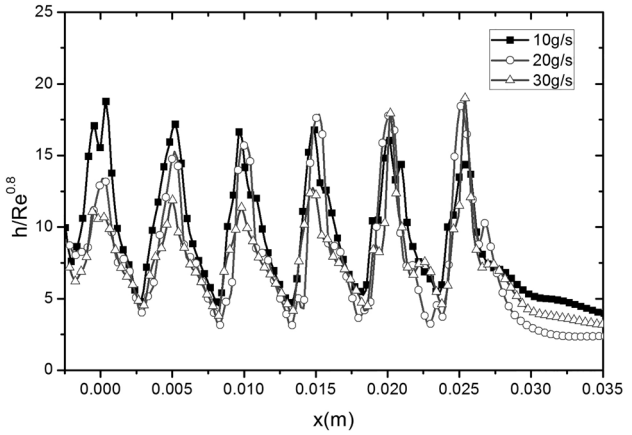

Fig. 15 Distributions of Heat transfer ratio along line *C* with different inlet mass flow rates

Table 2 The comparison of pressure loss with different inlet mass flow

	$\dot{m} = 10\,\mathrm{g/s}$	$\dot{m} = 20\,\mathrm{g/s}$	$\dot{m} = 30\,\mathrm{g/s}$
ΔP (kPa)	8.7	29	60

[22]. Table 2 shows the pressure loss of the impingement system for different inlet mass flow rates. One can see that increasing inlet mass flow rate causes larger pressure loss since the kerosene velocity increases with the mass flow rate.

4.4 Effects of Inlet Temperature. For air impingement cooling, heat transfer characteristics of the flow are nearly independent on inlet temperature. Fan et al. [31] indicated that kerosene jet structures at varying preheat temperatures with a fixed injection pressure are quite different since the thermophysical properties of kerosene are essentially different at varied temperatures. Distributions of heat transfer coefficient at varied inlet temperatures on the target wall are shown in Fig. 16. One can see that the heat transfer rates increase first with the increasing of inlet temperature and then decrease suddenly when the inlet temperature is 500 K. The kerosene flow in the vicinity of the target wall is significantly heated by the hot wall and its temperature approaches the wall temperature. For the case of inlet temperature of 500 K, the local temperature on the target plate is nearly 600–700 K between the adjacent jets as shown in Fig. 17. It is known that as the wall temperature is close to the pseudo-critical temperature of kerosene, heat transfer deterioration occurs [7,8]. The deterioration of heat transfer is related to the local wall temperature. The heat transfer

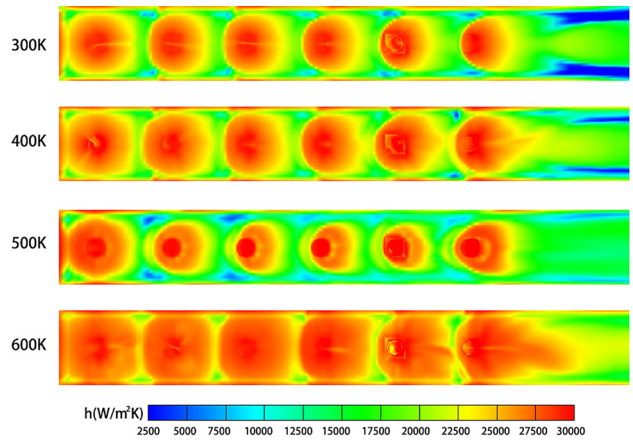

Fig. 16 The heat transfer distributions on the target wall for different inlet temperatures

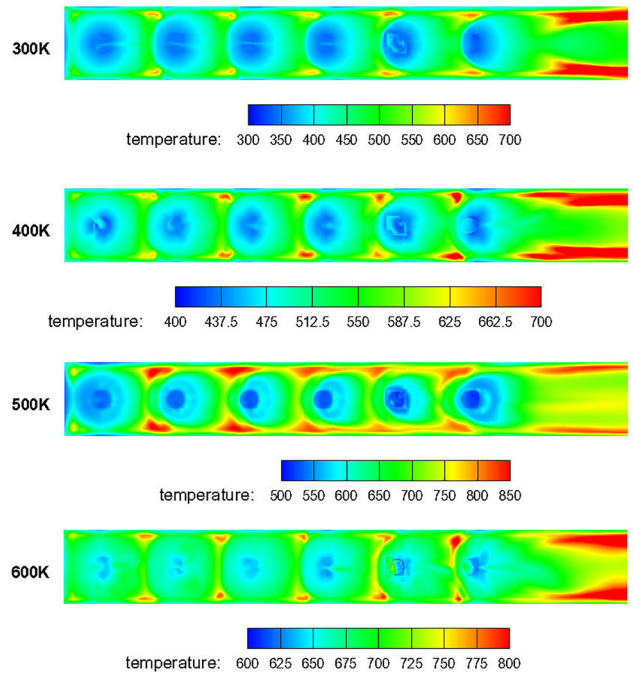

Fig. 17 The local temperature distribution on the target plate with different inlet temperatures

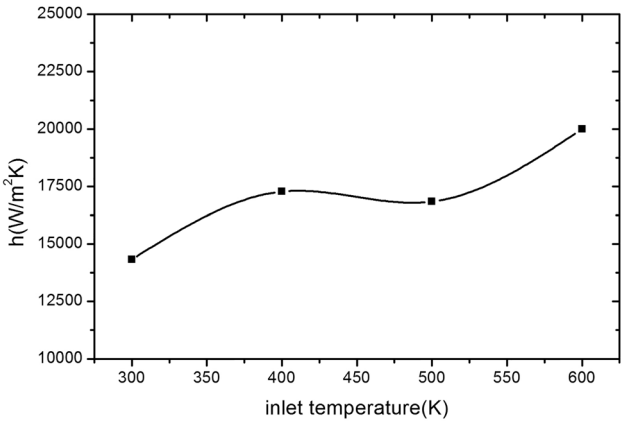

Fig. 18 The total averaged heat transfer coefficients on the target plate for different inlet temperatures

Table 3 The comparison of pressure loss with different inlet temperature

	300 K	400 K	500 K	600 K
ΔP (kPa)	7.0	8.7	8.6	9.0

rates increase again when the local wall temperature is over 700 K. Figure 18 shows the total averaged heat transfer coefficients on the target plate with different inlet temperatures. The heat transfer coefficients increase with increasing inlet temperature, but there is heat transfer deterioration at inlet temperature 500 K. Table 3 shows the pressure loss of the impingement system for different inlet temperature. Increasing inlet temperatures cause decreasing local density and increasing fuel velocity that lead to larger pressure loss.

5 Conclusions

In the present paper, numerical study of flow and heat transfer properties of RP-3 kerosene at supercritical conditions in an impingement model is conducted with RNG $k-\varepsilon$ turbulence model and a ten-species surrogate of kerosene. The independence of grids is first studied and the numerical results are compared with experimental data for validation. Characteristics of flow and heat transfer of kerosene flow in the impingement model are studied with different inlet mass flow and different inlet temperature. The velocity and temperature field shows similar profile compared to that of air impingement. And the impingement enhances the heat transfer on the target wall significantly compared to a straight pipe. The higher mass flow rate causes higher heat transfer rates on the target wall. The deterioration of convective heat transfer occurs at inlet temperature 500 K for the present impingement configuration.

Funding Data

- The National Natural Science Foundation of China (Grant Nos. 11672307 and 11202218).
- The Youth Innovation Promotion Association CAS.

Nomenclature

C_d = discharge coefficient
d = diameter of the jets, m
G_{cf} = channel crossflow velocity, m/s
G_j = jet velocity, m/s
h = heat transfer coefficient, W/m^2 K
H = height of the impinging jet
k = thermal conductivity, W/m K
$L1/L2$ = width and length of the target wall, m
$\dot{m}$ = mass flow rate, g/s
Q = heat flux on the target plate, MW/m^2
Re = Reynolds number
S = distance of the adjacent jets, m
T_f = inlet temperature, K
T_w = wall temperature, K
u = bulk velocity, m/s
ρ = density, kg/m^3

References

[1] Hendricks, R. C., Simoneau, R. J., and Smith, R. V., 1970, "Survey of Heat Transfer to Near-Critical Fluids," National Aeronautics and Space Administration, Washington, DC, Technical Note No. NASA-TN-D-5886.
[2] Bellan, J., 2000, "Supercritical (Subcritical) Fluid Behavior and Modeling: Drops, Streams, Shear and Mixing Layers, and Sprays," Prog. Energy Combust. Sci., **26**(4–6), pp. 329–366.
[3] Yang, V., 2000, "Modeling of Supercritical Vaporization, Mixing and Combustion Processes in Liquid-Fueled Propulsion System," Proc. Combust. Inst., **28**(1), pp. 925–942.

[4] Linne, D. L., and Meyer, M. L., 1997, "Evaluation of Heat Transfer and Thermal Stability of Supercritical JP-7 Fuel," AIAA Paper No. 97-3041.
[5] Hu, Z. H., Chen, T. K., and Luo, Y. S., 2002, "Heat Transfer to Kerosene at Supercritical Pressure in Small-Diameter Tube With Large Heat Flux," J. Chem. Ind. Eng., **53**(2), pp. 134–138.
[6] Zhong, F., Fan, X., Yu, G., Li, J., and Sung, C.-J., 2009, "Heat Transfer of Aviation Kerosene at Supercritical Conditions," J. Thermophys. Heat Transfer, **23**, pp. 543–550.
[7] Dang, G., Zhong, F. Q., Zhang, Y. J., and Zhang, X. Y., 2015, "Numerical Study of Heat Transfer Deterioration of Turbulent Supercritical Kerosene Flow in Heated Circular Tube," Int. J. Heat Mass Transfer, **85**, pp. 1003–1011.
[8] Wang, X., Zhong, F. Q., Chen, L. H., and Zhang, X. Y., 2013, "A Coupled Heat Transfer Analysis With Effects of Catalytic Cracking of Kerosene for Actively Cooled Supersonic Combustor," J. Propul. Technol., **34**(1), pp. 47–53.
[9] Buchlin, J.-M., 2000, "Convective Heat Transfer in Impinging Gas-Jet Systems," Lecture Series 2000–03, von Karman Institute for Fluid Dynamics, Rhode Saint Genese, Belgium, pp. 1–33.
[10] Han, B., and Goldstein, R., 2000, "Aero-Thermal Performance of Internal Cooling Systems in Turbomachines," Lecture Series 2000–03, von Karman Institute for Fluid Dynamics, Rhode Saint Genese, Belgium, pp. 34–57.
[11] Chambers, A., Gillespie, D., Ireland, P., and Mitchell, M., 2006, "Enhancement of Impingement Cooling in a High Cross Flow Channel Using Shaped Impingement Cooling Holes," ASME Paper No. GT2006-91229.
[12] Son, C., Gillespie, D., Ireland, P., and Dailey, G., 2001, "Heat Transfer and Flow Characteristics of an Engine Representative Impingement Cooling System," ASME J. Turbomach., **123**(1), pp. 154–160.
[13] Gao, L., 2003, "Effect of Jet Hole Arrays Arrangement on Impingement Heat Transfer," M.Sc. thesis, The Louisiana State University, Baton Rouge, LA.
[14] Lee, D. H., Song, J., and Jo, M. C., 2004, "The Effects of Nozzle Diameter on Impinging Jet Heat Transfer and Fluid Flow," ASME J. Heat Transfer, **126**, pp. 554–557.
[15] San, J. Y., and Shiao, W. Z., 2006, "Effects of Jet Plate Size and Plate Spacing on the Stagnation Nusselt Number for a Confined Circular Air Jet Impinging on a Flat Surface," Int. J. Heat Mass Transfer, **49**(19–20), pp. 3477–3486.
[16] Martin, H., 1977, "Heat and Mass Transfer Between Impinging Gas Jets and Solid Surfaces," Adv. Heat Transfer, **13**, pp. 1–60.
[17] Han, B., and Goldstein, R.-J., 2001, "Jet-Impingement Heat Transfer in Gas Turbine Systems," Ann. N. Y. Acad. Sci., **934**(1), pp. 147–161.
[18] Jambunathan, K., Lai, E., Moss, M., and Button, B., 1992, "A Review of Heat Transfer Data for Single Circular Jet Impingement," Int. J. Heat Fluid Flow, **13**(2), pp. 106–115.
[19] Weigand, B., and Spring, S., 2009, "Multiple Jet Impingement—A Review," Heat Transfer Res., **42**(2), pp. 101–142.
[20] Zhong, F. Q., Fan, X. J., Yu, G., Li, J. G., and Sung, C. J., 2011, "Thermal Cracking and Heat Sink Capacity of Aviation Kerosene Under Supercritical Conditions," J. Thermophys. Heat Transfer, **25**(3), pp. 450–456.
[21] Wolfstein, M., 1969, "The Velocity and Temperature Distribution of One-Dimensional Flow With Turbulence Augmentation and Pressure Gradient," Int. J. Heat Mass Transfer, **12**(3), pp. 301–318.
[22] Xing, Y., Spring, S., and Weigand, B., 2010, "Experimental and Numerical Investigation of Heat Transfer Characteristics of Inline and Staggered Arrays of Impinging Jets," ASME J. Heat Transfer, **132**(9), p. 092201.
[23] Katti, V., and Prabhu, S., 2008, "Influence of Spanwise Pitch on Local Heat Transfer Distribution for In-Line Arrays of Circular Jets With Spent Air Flow in Two Opposite Directions," Exp. Therm. Fluid Sci., **22**(1), pp. 84–95.
[24] Baughn, J. W., Hechanova, A. E., and Yan, X., 1991, "An Experimental Study of Entrainment Effects on the Heat Transfer From a Flat Surface to a Heated Circular Impinging Jet," ASME J. Heat Transfer, **113**, pp. 1023–1025.
[25] Florschuetz, L. W., Truman, C. R., and Metzger, D. E., 1981, "Streamwise Flow and Heat Transfer Distributions for Jet Array Impingement With Crossflow," ASME J. Heat Transfer, **103**, pp. 337–342.
[26] Bailey, J. C., and Bunker, R. S., 2002, "Local Heat Transfer and Flow Distributions for Impinging Jet Arrays of Dense and Sparse Extent," ASME Paper No. GT-2002-30473.
[27] Annerfeldt, M. O., Persson, J. L., and Torisson, T., 2001, "Experimental Investigation of Impingement Cooling With Turbulators or Surface Enlarging Elements," ASME Paper No. 2001-GT-0149.
[28] Terzis, A., 2006, "On the Correspondence Between Flow Structures and Convective Heat Transfer Augmentation for Multiple Jet Impingement," Exp. Fluids, **57**(9), p. 146.
[29] Florschuetz, L. W., and Isoda, Y., 1983, "Flow Distributions and Discharge Coefficient Effects for Jet Array Impingement With Initial Crossflow," J. Eng. Power, **152**(2), pp. 296–304.
[30] Florschuetz, L. W., Metzger, D. E., and Truman, C. R., 1981, "Jet Array Impingement With Crossflow-Correlation of Streamwise Resolved Flow and Heat Transfer Distributions," National Aeronautics and Space Administration, Washington, DC, Report No. NASA-CR-3373.
[31] Fan, X. J., Yu, G., Li, J. G., and Zhang, X. Y., 2006, "Investigation of Vaporized Kerosene Injection and Combustion in a Supersonic Model Combustor," J. Propul. Power, **22**(1), pp. 103–110.